Наносистеми, наноматеріали, нанотехнології
Nanosistemi, Nanomateriali, Nanotehnologii
2017, т. 15, № 3, сс. 401–416

PACS numbers: 61.05.cp, 61.43.Gt, 61.68.+n, 68.37.Hk, 81.07.Wx, 81.20.Ev, 81.20.Wk

Microstructure Characterization of Nanocrystalline $Ni_{50}Ti_{50}$ Alloy Prepared *Via* Mechanical Alloying Method Using the Rietveld Refinement Method Applied to the X-Ray Diffraction

E. Sakher[1,3], N. Loudjani[2], M. Benchiheub[3], S. Belkahla[3], and M. Bououdina[4,5]

[1]*Laboratoire de physique des solides,*
Department of Physics, Faculty of Science,
University Badji Mokhtar,
Annaba, Algeria
[2]*Laboratoire de Microstructures et Defauts,*
Department of Physics, Faculty of Science,
University of Mentouri,
Constantine, Algeria
[3]*Laboratoire d'Elaboration et d'Analyse des Materiaux LEAM,*
Department of Physics, Faculty of Science,
University Badji Mokhtar,
Annaba, Algeria
[4]*Nanotechnology Centre,*
University of Bahrain,
PO Box 32038, Zallaq, Kingdom of Bahrain
[5]*Department of Physics, College of Science,*
University of Bahrain,
PO Box 32038, Zallaq, Kingdom of Bahrain

Using the Rietveld refinement, we analysed the structural evolution of $Ni_{50}Ti_{50}$ alloy prepared by mechanical alloying method. The elemental Ti and Ni powders are milled during different milling times (0, 1, 3, 6, 24, and 72 hours) in a high-energy planetary ball mill (Pulverisette 7 premium line). The milled powder specimens were characterized with x-ray Philips X,Pert diffractometer equipped with CuK_α radiation source ($\lambda_{Cu} = 0.15418$ nm). We refined the structure of compounds using the MAUD program, and we found structural parameters such as the atomic positions (x, y, z), symmetry, and a space group. Moreover, microstructural parameters such as the lattice parameters (a, b, c), the average crystallite size $<L>$, microstrains $<\sigma_2>^{1/2}$, the average number of compacted layers, and the phase percentages were also determined. According to the results, at the initial stages of milling (typically of 1–3 h), the structure consists of Ni-based solid solution [f.c.c.-Ni (Ti)],

Ti-based solid solution [h.c.p.-Ti (Ni)], and amorphous phase (≅ 40 wt.%). Based on the data evaluated during milling, the nanocrystalline NiTi-martensite ($B19'$) and NiTi-austenite ($B2$) phases are initially formed from the primary materials and from the amorphous phase.

Використовуючи Рітвелдову методу повнопрофільної аналізи структури, ми аналізували структурну еволюцію стопу $Ni_{50}Ti_{50}$, підготовленого методою механічного леґування. Елементні порошки титану та ніклю мелються протягом різних часів здрібнювання (0, 1, 3, 6, 24 і 72 години) у високоенергетичному внутрішньошліфувальному планетарному кульовому млині тонкого млива (Pulverisette 7 преміяльної лінії). Намолочені порошкові зразки для випробування були охарактеризовані рентґенівським дифрактометром Philips X,Pert, обладнаним джерелом випромінення CuK_α (λ_{Cu} = 0,15418 нм). Ми уточнили будову сполук, використовуючи програму MUAD (аналізи матеріялів з використанням дифракції), і ми знайшли структурні параметри типу атомових позицій (x, y, z), симетрію та просторову групу. Крім того, мікроструктурні параметри типу параметрів ґратниці (a, b, c), середній розмір кристаліта $<L>$, мікродеформації $<\sigma_2>^{1/2}$, середнє число ущільнених шарів і фазові процентні вмісти були також визначені. Згідно з результатами, на початкових стадіях розмелювання (звичайно 1–3 години), структура складається із твердого розчину на основі ніклю [ГЦК-нікель (Ti)], твердого розчину на основі титану [ГЩП-титан (Ni)] і аморфної фази (≅ 40 ваг.%). Ґрунтуючись на даних, оцінених протягом розмелювання, з'ясовано, що нанокристалічні фази NiTi-мартенситу ($B19'$) і NiTi-аустеніту ($B2$) спочатку сформувалися з первинних матеріялів і з аморфної фази.

Используя ритвелдовский метод полнопрофильного анализа структуры, мы анализировали структурную эволюцию сплава $Ni_{50}Ti_{50}$, подготовленного методом механического легирования. Элементные порошки титана и никеля мелются в течение различных времён измельчения (0, 1, 3, 6, 24 и 72 часа) в высокоэнергетической внутришлифовальной планетарной шаровой мельнице тонкого помола (Pulverisette 7 премиальной линии). Намолоченные порошковые образцы для испытания были охарактеризованы рентгеновским дифрактометром Philips X,Pert, оборудованным источником излучения CuK_α (λ_{Cu} = 0,15418 нм). Мы уточнили строение соединений, используя программу MUAD (анализа материалов с использованием дифракции), и мы нашли структурные параметры типа атомных позиций (x, y, z), симметрию и пространственную группу. Кроме того, микроструктурные параметры типа параметров решётки (a, b, c), средний размер кристаллита $<L>$, микродеформации $<\sigma_2>^{1/2}$, среднее число уплотнённых слоёв и фазовые процентные содержания были также определены. Согласно результатам, на начальных стадиях размалывания (обычно 1–3 часа), структура состоит из твёрдого раствора на основе никеля [ГЦК-никель (Ti)], твёрдого раствора на основе титана [ГПУ-титан (Ni)] и аморфной фазы (≅ 40 вес.%). Основываясь на данных, оценённых в течение размалывания, выяснено, что нанокристаллические фазы NiTi-мартенсита ($B19'$) и NiTi-аустенита ($B2$) первоначально сформировались из первичных материалов и из аморфной фазы.

Key words: nanocrystalline materials, mechanical alloying, x-ray diffraction, microstructure, Rietveld refinement.

Ключові слова: нанокристалічні матеріяли, механічне леґування, рентґенівська дифракція, мікроструктура, Рітвелдова метода повнопрофільної аналізи.

Ключевые слова: нанокристаллические материалы, механическое легирование, рентгеновская дифракция, микроструктура, ритвелдовский метод полнопрофильного анализа.

(Received 10 July, 2017)

1. INTRODUCTION

In the last years, nanostructured materials are experiencing a growing interest because of their fascinating and unique physical properties often superior compared to the bulk materials of similar composition and due to the reduction of the grain size [1] and the large amount of interfaces. These materials present specific physical [2], mechanical [3], electrical [4], and magnetic properties [5]. Hence, new fields of technological application [1] are offered.

The excellent properties of NiTi, especially its advantageous mechanical and chemical properties such as superelasticity, a shape memory effect [6], a good corrosion resistance [7], a hydrogen storage ability and a good biocompatibility [8–9], which make this extraordinarily attractive material for the aeronautic and aerospace industries, the biomedical and dentistry applications [10], which demand half of all NiTi produced.

A number of different methods have been used to synthesize nanocrystalline/amorphous NiTi materials. These include an ion-milling deposition [11], a melt spinning [12], a high-pressure torsion [13], a conventional powder metallurgy [14], a self-propagating high-temperature synthesis, an explosive shock-wave compression [15], and mechanical alloying (MA) [2].

Among these, the MA method was very effective for the fabrication of $Ni_{50}Ti_{50}$ nanocrystalline alloys or nanostructured powders. In this technique, high-energy collisions between the milled powder particles, balls, and vial walls generate a large variety of materials such as a nanocrystalline solid solution amorphous phase [16], the NiTi-austenite ($B2$) and NiTi-martensite ($B19'$) phases [17].

Moreover, in this process, the reduction of particle size is observed that results in the ultrafine grained or nanocrystalline materials. Because of the very fine grain sizes, nanocrystalline materials exhibit a diversity of properties, which are different and often considerably improved in comparison with those of conventional coarse-

grained polycrystalline materials [18].

The Rietveld method, a full-pattern fit method for the microstructural characterization of materials, is the best method for the microstructure characterization and for the quantitative estimation of multiphase nanocrystalline materials containing significant number of overlapping reflections [19]. The Rietveld method was successfully applied for determination of microstructural properties of many different systems [1, 5, 10].

In the present work, the mechanical alloying in a high-energy planetary ball mill produces nanocrystalline $Ni_{50}Ti_{50}$ powders. The effects of the milling time on the microstructure and morphology of mechanically alloyed powder mixtures is studied by means of the x-ray diffraction (XRD) and scanning electron microscopy (SEM).

2. EXPERIMENTAL: SYNTHESIS OF THE ALLOYS

Elemental Ti and Ni powders (Aldrich) with purity of 99.97% and 99.99%, respectively, and with a particle size under 150 μm for Ti and under 45 μm for Ni were used. Powders were mixed to obtain the $Ni_{50}Ti_{50}$ (at.%) composition. Mechanical alloying performed under an argon atmosphere using the Fritsch Pulverisette P7 planetary ball mill equipped with hardened steel vial (80 mL) and balls (15 mm diameter) fabricate the $Ni_{50}Ti_{50}$ powders. The disk speed rotation was $\Omega = 400$ rpm. The ball-to-powder weight ratio was 23:1. The synthesis was performed by milling cycles of 30 min at 400 rpm and followed with equal rest periods (pauses of 30 min) to avoid an excessive rise of temperature inside the vials. The powders had milled for several periods including 0, 1, 3, 6, 24 and 72 h.

Changes in the morphology of the powder particles (changes in size and shape of the powder particles and their distribution) were determined by scanning electron microscopy (SEM) using a Zeiss DSM 960A microscope operating at a voltage of 20 kV.

X-ray diffraction patterns were recorded by the x-ray diffraction (XRD) method, using x-ray Philips X,Pert diffractometer equipped with CuK_α radiation source ($\lambda_{Cu} = 0.15418$ nm). The phase analysis was performed by application of ICDD (PDF-2, 2012) files. The microstructural parameters were taken from the refinement of the XRD patterns by using the MAUD program (version 2.55), which is based on the Rietveld method [20].

Using the Rietveld refinement and Warren–Averbach methods [21, 22] within the frame of the MAUD software [20], we can get a detailed analysis of the XRD profiles and extract structural parameters such as the atomic positions (x, y, z), symmetry, and space group. Moreover, microstructural parameters such as the lattice parameters (a, b, c), the average crystallite size $\langle L \rangle$, microstrains

$<\sigma_2>^{1/2}$, the average number of compacted layers, and the phase percentages were determined too.

From the values of a lattice parameter, the crystallite size and microstrains, the dislocation density (ρ) can be calculated using following formula:

$$\rho = 2\sqrt{3} < \sigma^2 >^{1/2} < L >^{-1} B_v^{-1},$$

where B_v is the Burgers vector module, which is equal to $a\sqrt{6}/3$ for the hexagonal close packed (h.c.p.) structure and $a\sqrt{2}/2$ for the face centred cubic (f.c.c.) structure.

The calculated profile yields scaling factors for each phase to fit the intensity of the observed pattern. These scale factors relate to the respective relative weight fractions by equation [23] as follows:

$$W_i = \frac{S_i (ZMV)_i}{\sum_{k=1}^{n} S_k (ZMV)_k},$$

where Z is the number of formula units in the unit cell, M is the molecular mass of the formula unit, V is the unit cell volume, S is the Rietveld scale factors, and W_i is the weight fraction of i-th phase; the index 'k' in the summation covers all phases, which are included in the model [23].

The weight percentage of the amorphous phase in a sample is given by the relationship [24]:

$$W_a = \frac{1}{1 - W_S}\left(1 - \frac{W_S}{W_R}\right),$$

where W_a is the amorphous fraction, W_S is the weighted internal standard fraction, and W_R is the refined fraction of the internal standard.

To evaluate the refinement, several factors have been introduced that make it possible to know the agreement between the calculated model and the observed model [23]. The minimization was carried out by using the reliability index parameters R_{wp} (a weighted residual error) and $R_{\exp}$ (an expected error) [19].

It is possible to calculate a statistical parameter, which must tend towards the unit for a successful refinement called the 'goodness of fit' χ^2, which is the ratio between R_{wp} and $R_{\exp}$:

$$\chi^2 = R_{wp} / R_{\exp}.$$

Profile refinement continues until convergence is reached in each case, with the value of the quality factor χ^2 (GOF) approaching one.

3. RESULTS AND DISCUSSION

3.1. Particle Morphology and Evolution Using SEM Analysis

Figure 1 shows the change of the morphological shape and the corresponding particles size distribution of the powders obtained after 0 h, 6 h, 24 h and 72 h of milling times. Morphological changes of $Ti_{50}Ni_{50}$ powder particles occurring during the mechanical milling of the starting mixture of elemental f.c.c.-Ni and h.c.p.-Ti can be related to the difference between the mechanical properties of metals. The unmilled Ni powder particles have roughly spherical and rounded shapes, while Ti possesses flake-like shape (Fig. 1, *a*). It can be seen that the morphology changes are great after 1 h of milling (Fig. 1, *b*). The particles are flattened by the plastic deformation caused by the progressive forces induced by the ball–powder–ball and ball–powder–vial contacts. This leads to increasing the size of particles beside some small particles produced [1].

By progression of milling (24 h), due to both the domination of fracturing over cold welding and the increase in the amorphous phase amount, the brittleness of powders increases. Consequently, the size of particles is appreciably reduced, and their morphology

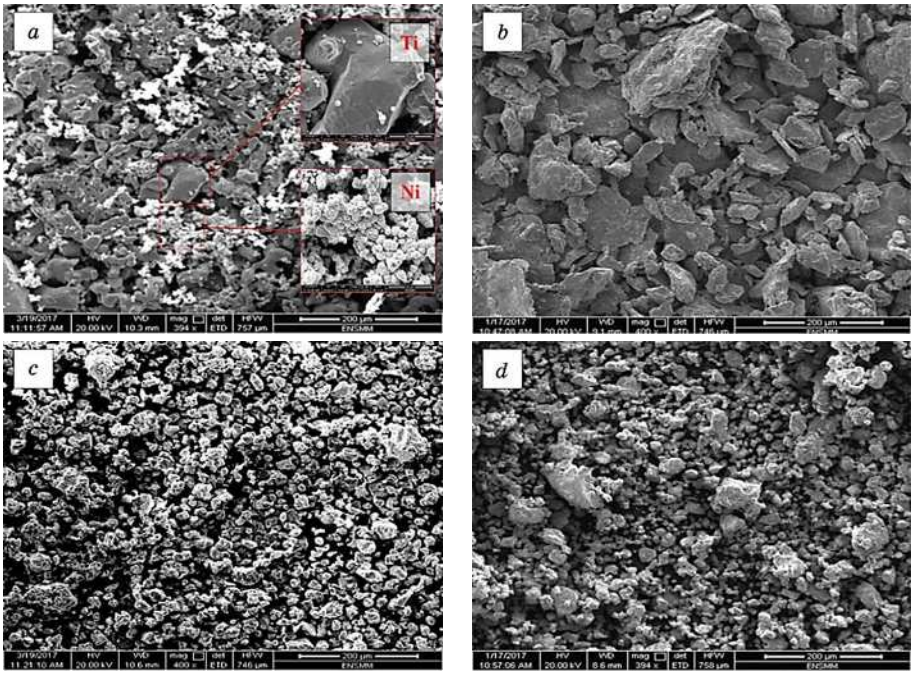

Fig. 1. SEM images of powders milled (*a*) 0 h, (*b*) 1 h, (*c*) 24 h, (*d*) 72 h.

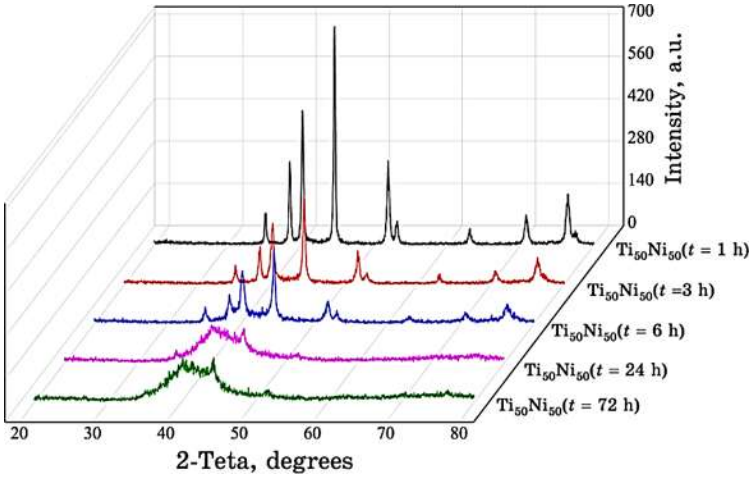

Fig. 2. XRD patterns of the $Ti_{50}Ni_{50}$ powders at different milling times.

tends to be semi-spherical with a narrow range of a size distribution (Fig. 1, *c*) [17].

The milling for 72 h leads to agglomeration of the smaller particles. Thus, the cold welding is the dominating phenomena at this stage of milling (Fig. 1, *d*).

3.2. Structural Analysis

The different diffractograms of $Ti_{50}Ni_{50}$ powders (after 0 h, 1 h, 3 h, 6 h, 24 h, and 72 h) are shown in Fig. 2. As is apparent, MA introduces significant changes in ground powders up to 72 hours.

There is a gradual increase in enlargement and a gradual decrease in intensity of different lines as functions of the milling time, illustrating the impact of the milling on the crushed powders. The superposition of lines shows an enlargement accompanied with a slight shift towards lower angles, indicating a slight increase in interatomic distances.

After a few hours of milling, one can see the appearance of halo around 35–50°, which is superimposed with peaks belonging to h.c.p.-Ti and f.c.c.-Ni, that could attribute to formation of an amorphous phase. The formation of such a structure can be explained by the significant structural disorder induced by the severe plastic deformation.

The best Rietveld refinements of the XRD patterns (1, 3, and 6 h) were obtained with three components: f.c.c.-Ni, h.c.p.-Ti, and an amorphous phase (Fig. 3, *a*, *b* and *c*). The nanometre-scaled diffusion couples are produced by high-energy mechanical milling, which

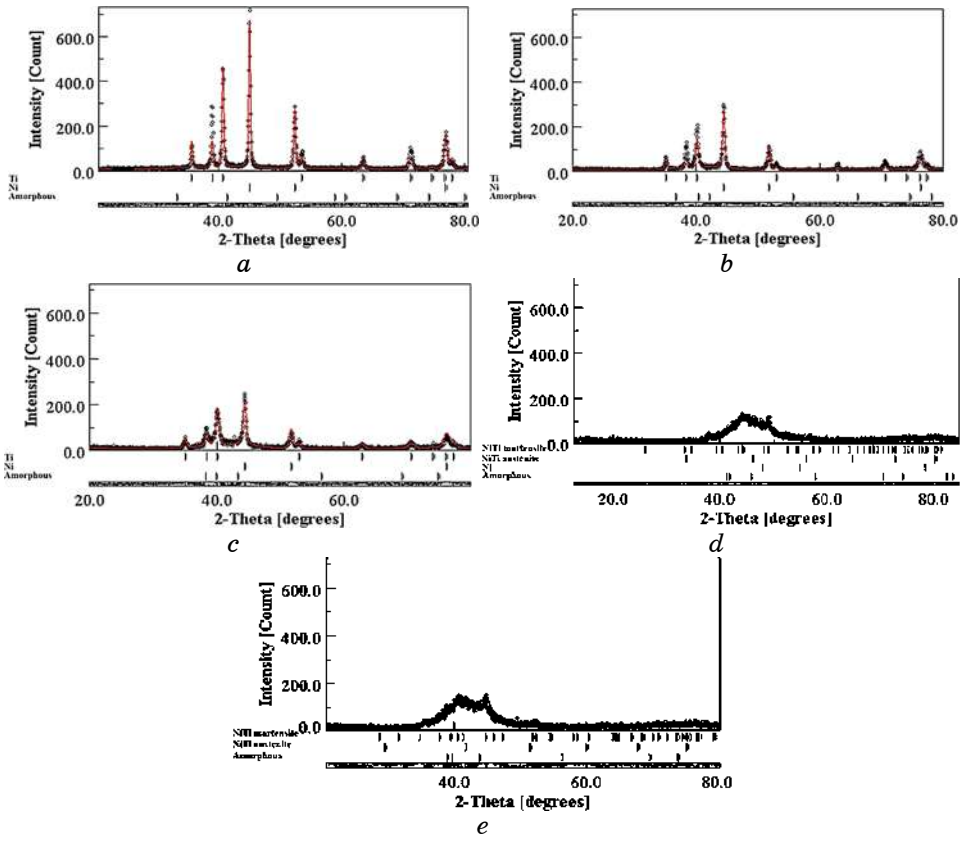

Fig. 3. Rietveld refinements of XRD patterns of the milled powders for: (*a*) 1 h (GOF = 1.41), (*b*) 3 h (GOF = 1.45), (*c*) 6 h (GOF = 1.43), (*d*) 24 h (GOF = 1.20), (*e*) 72 h (GOF = 1.23).

involves fracture and cold welding of milled powders. Thus, the atomic diffusivity is improved through the creation of a large amount of structural defects. As a result, metastable phases may be the first products of the solid-state reaction.

With further milling (24 h), the complete disappearance of the h.c.p.-Ti Bragg peaks, as evidenced by the absence of their peaks in the XRD pattern, is linked to the formation of *B*2 phase (Fig. 3, *d*), while the Ni-SS is still presented with very a few amounts (15.38%). Furthermore, it is known that the crystallite size decreases with the increase of negative mixing enthalpy (ΔH) [25].

After 72 h of milling, XRD patterns present the same phases, *B*2 and *B*19′, with the dominance of an amorphous phase (Fig. 3, *e*) with a relative proportion of about 68.9577%.

According to Rietveld refinements of XRD patterns of the milled

powders, we can extract all structural parameters (symmetry, space group, and atomic positions), variation of phases' content (in weight percentage), and goodness of fit (as shown in Table 1).

In order to investigate the phases' stabilities during mechanical milling, we have calculated the phase proportions of the identified phases as functions of milling times. The obtained results are presented in Table 1. At the early stages of milling, the fractions of mixed elements are decreased. This is due to the continuous dissolution of phases and solid solution formation.

During the stage of 1–6 h, which represents a post-formation of an amorphous phase, we note that decreasing ratios of titanium and nickel is inversely proportional to the ratio of an amorphous phase and increasingly very clear.

After 24 h, it is the stage, which starts the formation of martensitic phases. We note here that the percentages of initial elements remain constantly waiver up to the total disappearance for h.c.p.-Ti. In addition, the $B19'$ and amorphous phases up to 24 h of milling continue to grow. The formation of martensitic phase may be due to the negative mixing enthalpy ($\Delta H = -67$ kJ/mol) [25].

After 72 h observing, the continued rise of both $B19'$ and $B2$ phases was due to a decline in the proportion of amorphous phase. The martensitic and austenitic phases were formed at the milling times of 24 h and 72 h due to severe plastic deformation. This is similar to that reported for the Ni–50Ti alloy [17].

We note that there is a change in the positions of atoms of all phases. As is evident for primary elements, they are constantly changing and increasing for f.c.c.-Ni and remain almost constant for h.c.p.-Ti. This may be explained by the dissolution of h.c.p.-Ti into f.c.c.-Ni to form solid solutions.

3.3. Microstructural Analysis

The variations in the average crystallite size $<L>$ and microstrains $<\sigma^2>^{1/2}$ obtained from Rietveld analysis are plotted as functions of milling time in Fig. 4. As shown, one can observe an important decrease in the crystallite size, when the microstrain of both Ni and Ti is increasing during the first stage of milling [I] (0–6 h).

Above-mentioned changes can be explained by the fact that the mechanical energy communicates during grinding and is sufficient to deform plastically the two elemental Ni and Ti powders.

At the second stage [II] between 6 and 24 h, the crystallite size becomes less dependent on the milling time. This stage precedes the $B19'$ appearance and can be the reason for lower decrease of a crystallite size. $B19'$ is characterized by a smaller crystallite size and higher microstrains in comparison with the first stage of milling.

TABLE 1. The structural parameters (symmetry, space group, and atomic positions), variation of phases' content (weight percentage), and goodness of fit.

Milling time (h) / Phases' proprieties				0 h	1 h	3 h	6 h	24 h	72 h
f.c.c.-Ni	Symmetry			Face Centred Cubic (f.c.c.)					
	Space group			$Fm\text{–}3m$					
	Atomic positions		x	0	$3.6514 \cdot 10^{-4}$	$-3.7125 \cdot 10^{-13}$	$-9.7524 \cdot 10^{-5}$	$-9.7093 \cdot 10^{-8}$	/
			y	0	$-8.8563 \cdot 10^{-5}$	$3.8032 \cdot 10^{-14}$	$-9.7523 \cdot 10^{-5}$	$-9.4076 \cdot 10^{-8}$	/
			z	0	$-5.9118 \cdot 10^{-5}$	$3.8032 \cdot 10^{-14}$	$-9.7523 \cdot 10^{-5}$	$-9.4076 \cdot 10^{-8}$	/
	Weight percent (%)			50	44.6675	39.4754	33.5159	15.3809	/
h.c.p.-Ti	Symmetry			Hexagonal Close Packed (h.c.p.)					
	Space group			$P63/mmc$					
	Atomic positions		x	0.3333	0.3328	0.3330	0.3328	/	/
			y	0.6667	0.6666	0.6664	0.6666	/	/
			z	0.2500	0.2497	0.25	0.2495	/	/
	Weight percent (%)			50	33.3126	20.6052	15.6617	/	/
$B19'$	Symmetry			Monoclinic					
	Space group			$P21/m{:}b$					
	Atomic positions	Ni	x	/	/	/	/	0.1987	0.0300
			y	/	/	/	/	0.7498	0.7505
			z	/	/	/	/	0.0509	–0.2475
		Ti	x	/	/	/	/	0.3150	0.3560
			y	/	/	/	/	0.2499	0.2497
			z	/	/	/	/	0.5174	0.8833
	Weight percent (%)			/	/	/	/	9.0527	21.5850

(Continuation) **TABLE 1.**

Milling time (h) Phases' proprieties				0 h	1 h	3 h	6 h	24 h	72 h
B2	Symmetry			Body Centred Cubic (b.c.c.)					
	Space group			*Pm*–3*m*					
	Atomic positions	Ni	*x*	/	/	/	/	$2.6461 \cdot 10^{-4}$	$5.3103 \cdot 10^{-5}$
			y	/	/	/	/	$-9.1927 \cdot 10^{-5}$	$-1.8236 \cdot 10^{-5}$
			z	/	/	/	/	$4.0825 \cdot 10^{-4}$	$4.4022 \cdot 10^{-4}$
		Ti	*x*	/	/	/	/	0.4996	0.4999
			y	/	/	/	/	0.5005	0.5004
			z	/	/	/	/	0.5005	0.4997
	Weight percent (%)			/	/	/	/	0.4372	9.4574
Amorphous	Weight percent (%)			/	22.0199	39.9194	50.8224	75.1292	68.9577
	GOF			1.11	1.41	1.45	1.43	1.20	1.23

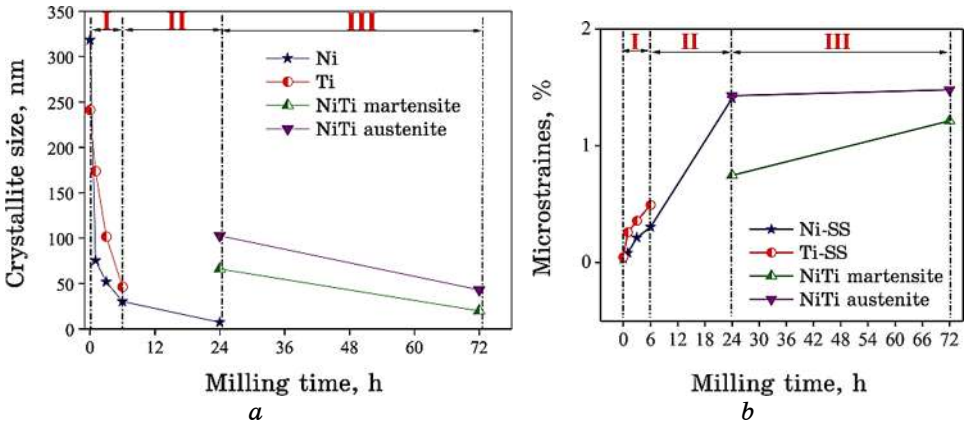

Fig. 4. The milling-time-dependent average crystallite size <*L*> (*a*) and microstrains $<\sigma^2>^{1/2}$ (*b*).

During the third stage [III] after 72 h, one can observe a decrease in crystallite size and an important increase in the microstrains of *B*19′ and *B*2, when the strains of the austenite phase are higher in comparison with the martensite. It could be due to high concentration of stacking faults and high dislocation density. Actually, the austenite phase is metastable at room temperature and becomes unstable when an external mechanical or thermal energy is introduced.

The reduction in crystallite size is mainly due to severe deformation of powders during the milling. The other reason can be increased probability of nucleation sites during crystallization, provided by higher defect densities [18].

The final crystallite size is in order of 7.1777 nm for f.c.c.-Ni and 29.0578 nm for h.c.p.-Ti. It is also evident that the decline in Ni crystallite size is faster than in Ti one, and this is probably related to a low initial grain size of f.c.c.-Ni (under 45 μm) compared with the grain size of h.c.p.-Ti (under 150 μm) [26].

*B*2 is characterized by higher microstrains (1.4788%) comparatively to *B*19′ (1.2132%) and may be due to high concentration of stacking faults and a high dislocation density. Generally, magnitudes of microstrains achieved during a milling are of about 1.5% [18].

Table 2 shows the variations of lattice parameters and the relative deviation of f.c.c.-Ni, h.c.p.-Ti, *B*2 and *B*19′ for each grinding time (0–72 h) as obtained from Rietveld analysis.

The decrease of the lattice parameters of f.c.c.-Ni (Ti) and h.c.p.-Ti (Ni) after 1 hour of milling is probably due to distortions of a crystal lattice resulting from the severe plastic deformation [19], and therefore, reducing the distance between neighbouring atoms.

TABLE 2. Variations of lattice parameters and the relative deviation of f.c.c.-Ni, h.c.p.-Ti, *B*2 and *B*19′ for each grinding time (0–72 h) as obtained from Rietveld analysis.

Milling time, h	f.c.c.-Ni		h.c.p.-Ti			*B*2		*B*19′				
	a, nm	$\Delta a/a_0$, %	*a*, nm	$\Delta a/a_0$, %	*b*, nm	$\Delta b/b_0$, %	*a*, nm	$\Delta a/a_0$, %	*a*, nm	$\Delta a/a_0$, %	*b*, nm	$\Delta b/b_0$, %	*c*, nm	$\Delta c/c_0$, %
0	0.3524	/	0.2952	/	0.4686	/	/	/	/	/	/	/	/	/
1	0.3527	0.0284	0.2947	1.3969	0.4677	0.2207	/	/	/	/	/	/	/	/
3	0.3534	0.1701	0.2953	1.6034	0.4687	0.4350	/	/	/	/	/	/	/	/
6	0.3520	0.2268	0.2956	1.7066	0.4688	0.4564	/	/	/	/	/	/	/	/
24	0.3574	1.3039	/	/	/	/	0.3134	3.9469	0.4534	1.9039	0.4376	3.9430	0.2952	2.3224
72	/		/		/	/	0.3045	0.9950	0.4687	1.4063	0.4238	0.6651	0.2942	1.9757

As well as partial dissolution of Ti atoms within the f.c.c.-Ni crystal lattice (h.c.p.-Ti atomic radius is slightly higher than that of f.c.c.-Ni), the progressive dissolution of Ti into f.c.c.-Ni lattice leads to increase of f.c.c.-Ni lattice parameter from 0.3524 nm to 0.3574 nm after 24 h of milling. However, the h.c.p.-Ti lattice parameter is reduced up to 1 h of milling, and then, the rest is continuing to rise, but in very small values. This low variance is due to the crystallite size reduction, the increase in rate of microdeformations, and a crystal-lattice distortion induced by the milling process.

The austenite-phase lattice parameter increases up to 72 h, when it reaches a value equal to $a = 0.3045$ nm and the $B19'$ lattice parameter values equal to $a = 0.4687$ nm, $b = 0.4238$ nm, $c = 0.2942$ nm.

The lattice-parameter relative deviation is increasing as a function of the milling time for Ni up to $\Delta a/a_0 = 1.3039\%$ after 24 h and Ti up to $\Delta a/a_0 = 1.7066\%$ and $\Delta b/b_0 = 0.4564\%$ after 6 h. However, it decreases for the austenite ($\Delta a/a_0 = 0.9950\%$) and martensite ($\Delta a/a_0 = 1.4063\%$, $\Delta b/b_0 = 0.6651\%$ and $\Delta c/c_0 = 1.9757\%$) phases after 72 h of milling. We can explain this because both phases tend to more stability with milling time. This high value can be associated with the severe plastic deformation, which introduces different types of defects such as dislocations, grain boundaries, gaps, and stacking faults, and it can be explained by the formation of a non-stoichiometric composition of an austenite phase.

The average number (N) of compacted layers between two stacking faults, either deformation or twin-type, is according to Warren's formula [27] as follows: $N = 1/SFP = 1/\left[1.5\left(\alpha' + \alpha''\right) + \beta\right]$, where α', α'' are the intrinsic and extrinsic deformation faults, re-

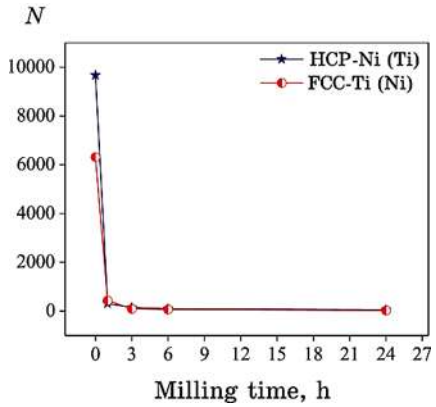

Fig. 5. Variation of the average number (N) of compacted layers between two stacking faults, either deformation or twin-type for the $Ni_{50}Ti_{50}$ powders as a function of milling time.

spectively, and β is the twin faults. The values of N decrease with the milling time (Fig. 5). In fact, there are 27 and 52 ordered planes between the two consecutive stacking faults in h.c.p.-Ti (Ni) and f.c.c.-Ni (Ti) after 24 of milling, respectively.

As clear, the value of the average number of compacted layers between two stacking faults in h.c.p.-Ti (Ni) is more than in the f.c.c.-Ni (Ti). Thus, it can explain that the h.c.p.-Ti (Ni) facilitate the formation of an amorphous phase more than the f.c.c.-Ni (Ti), while the f.c.c.-Ni participate in the formation of the $B19'$ and $B2$ phases.

4. CONCLUSION

The $Ni_{50}Ti_{50}$powders have been synthesized by mechanical milling for various milling durations and characterized with the Rietveld refinement method applied to the x-ray diffraction. The results are summarized as follows:

at the initial stages of milling, the elemental powders are dissolved into the structure, in which the Ti peaks are diminished faster than Ni peaks;

the best Rietveld refinement with the quality factors of fitting, namely GOF = 1.20, was subsequently performed with the following phases: $B19'$, $B2$, and an amorphous phase characterized by the low crystallite-size and microstrain rate (almost zero);

the amorphization process is occurred and the amorphous phase fraction is increased reaching its maximum value (≅ 75 wt.%) at 24 h of milling;

the nanocrystallization is developed at short milling, and the crystallite size decreases down to the nanometre scale (≅ 8nm) after 72 h of milling;

for prolonged milling time (24 h), the increase of stacking faults in h.c.p.-Ti (Ni) and f.c.c.-Ni (Ti) leads to the $B19'$ and $B2$ phases due to crystallite-size refinement down to the nanometre scale and large internal strains, and stacking faults incorporated in the f.c.c.-Ni (Ti) and h.c.p.-Ti (Ni) lattices;

the relative deviation of the lattice parameter is increasing as a function of the milling time for f.c.c.-Ni (Ti) and h.c.p.-Ti (Ni), but it decreases for the $B2$ and $B19'$ phases after 72 h of milling.

REFERENCES

1. N. Loudjani, M. Benchiheub, and M. Bououdina, *J. Supercond Nov. Magn.*, **29**: 2717 (2016).
2. M. Akmal, A. Raza, M. Mudasser, M. I. Khan, and M. A. Hussain, *Materials Science and Engineering C*, **68**: 30 (2016).

3. F. Alvarado-Hernández, O. Jiménez, G. González-Castaceda, V. Baltazar-Hernández, J. Cabezas-Villa, M. Albiter, H. Vergara-Hernández, and L. Olmos, *Transactions of Nonferrous Metals Society of China*, **26**, Iss. 8: 2126 (2016).
4. C. Murugesan, M. Perumal, and G. Chandrasekaran, *Physica B*, **448**: 53 (2014).
5. N. Loudjani, N. Bensebaa, L. Dekhil, S. Alleg, and J. J. Sucol, *Journal of Magnetism and Magnetic Materials*, **323**: 3063 (2011).
6. J. P. Oliveira, F. M. Braz Fernandes, N. Schell, and R. M. Miranda, *Materials Letters*, **171**: 273 (2016).
7. M. Karbasi, M. R. Zamanzad Ghavidel, and A. Nekahi, *Materials and Corrosion*, **65**, Iss. 5: 485 (2014).
8. C. H. Ng, Nanxi Rao, W. C. Law, G. Xu, T. L. Cheung, F. T. Cheng, X. Wang, and H. C. Man, *Surface & Coatings Technology*, **309**: 59 (2017).
9. J. Sevcikova and M. P. Goldbergova, *BioMetals*, **30**, No. 2: 163 (2017).
10. M. Karolus and J. Panek, *Journal of Alloys and Compounds*, **658**: 709 (2016).
11. K. Ashvani, S. Devendra, K. Ravi, and K. Davinder, *Journal of Alloys and Compounds*, **479**: 166 (2009).
12. K. Mehrabi, M. Bruncko, B. J. McKay, and A. C. Kneissl, *Journal of Materials Engineering and Performance*, **18**: 5 (2009).
13. T. Leitner, I. Sabirov, R. Pippan, and A. Hohenwarter, *Journal of the Mechanical Behavior of Biomedical Materials*, **71**: 337 (2017).
14. F. Neves, F. M. Braz Fernandes, and J. B. Correia, *Materials Science Forum*, **636–637**: 544 (2010).
15. Y. W. Gu, C. W. Goh, L. S. Goi, C. S. Lim, A. E. W. Jarfors, B. Y. Tay, and M. S. Yong, *Materials Science and Engineering A*, **392**, Iss. 1: 222 (2005).
16. T. Mousavi, F. Karimzadeh, and M. H. Abbasi, *Materials Science and Engineering A*, **487**: 46 (2008).
17. R. Amini, F. Alijani, M. Ghaffari, M. Alizadeh, and A. K. Okyay, *Powder Technology*, **253**: 797 (2014).
18. C. Suryanarayana, *Materials Science and Engineering A*, **479**: 23 (2008).
19. H. Dutta, A. Sen, J. Bhattacharjee, and S. K. Pradhan, *Journal of Alloys and Compounds*, **493**: 666 (2010).
20. L. Lutterotti, *Microstructure Analysis by MAUD* (2016); http://maud.radiographema.com/.
21. B. E. Warren and B. L. Averbach, *J. Appl. Phys.*, **21**: 595 (1950).
22. H. M. Rietveld, *J. Appl. Crystallogr.*, **2**: 65 (1969).
23. R. J. Hill, *Powder Diffraction*, **6**: 74 (1991).
24. R. Amini, M. J. Hadianfard, E. Salahinejad, M. Marasi, and T. Sritharan, *J. Mater. Sci.*, **44**: 136 (2009).
25. B.-Y. Li, L.-J. Rong, and Y.-Y. Li, *Intermetallics*, **8**: 643 (2000).
26. W. Maziarz, J. Dutkiewicz, J. Van Humbeeck, and T. Czeppe, *Materials Science and Engineering A*, **375–377**: 844 (2004).
27. J. Sort, J. Nogués, S. Suricach, J. S. Mucoz, and M. D. Bary, *Materials Science and Engineering A*, **377**: 869 (2004).